Rheology of Poly(ethylene oxide)/Organoclay Nanocomposites

Yang H. Hyun, Sung T. Lim, Hyoung J. Choi,*,† and Myung S. Jhon‡

Department of Polymer Science and Engineering, Inha University, Inchon, 402-751, Korea, and Department of Chemical Engineering, Carnegie Mellon University, Pittsburgh, Pennsylvania 15213-3890

Received December 26, 2000

ABSTRACT: A series of poly(ethylene oxide) (PEO)/organoclay nanocomposites have been prepared via a solvent casting method. Using three different organoclays modified with the alkylammonium salts, the effect of surfactants on organoclay surfaces in polymer/organoclay nanocomposites was investigated by focusing on two major aspects: internal structure analysis and rheological measurement of the nanocomposites. The *d* spacings of both the pure PEO and intercalated organoclay were examined via X-ray diffraction analysis, and the microstructure of these nanocomposites was examined by transmission electron microscopy. Rheological properties of these nanocomposites exhibited different behavior with different modifier concentrations and surfactant sizes (chain lengths). To analyze the non-Newtonian flow behavior, we fitted shear viscosity data via the Carreau model, showing that steady shear viscosity and power-law behavior increase with organoclay content. Hysteresis phenomenon was also enhanced with organoclay content, and the increase in the storage/loss moduli and interactions among organoclay platelets were observed with organoclay content. The enhanced thermal stability of the nanocomposites by organoclay was also observed.

Introduction

Nanostructured, hybrid organic/inorganic composites have recently attracted considerable attention, as researchers strive to enhance material properties via nanoscale reinforcement in contrast to the conventional particulate filled, microcomposites.[1,2] Clays, having a large aspect ratio and size, have been recognized as potential candidates for filler materials, because they exhibit superior physical and mechanical properties when compared with the pure polymer or conventional composites. These include improved moduli and optical properties, increased heat resistance,[3] and decreased gas permeability and flammability. Recently, Gilman and co-workers[4−6] have found that polymer layered-silicate (clay) nanocomposites have the unique combination of reduced flammability and improved physical properties. In other applications, polymer/clay nanocomposites prepared from an emulsion polymerization with polyaniline[7] and styrene−acrylonitrile copolymer[8] have also been adopted for clay-based electrorheological (ER) fluids. ER fluids consist of the suspension of dispersed, polarizable solid particles in an insulating liquid, which exhibit drastic and reversible changes in their rheological properties via their ordering of particles into columns[9,10] when an external electric field is applied. Recently, preparation methods for polymer/clay nanocomposites have been focused on the molecular-level architecture of the layered silicate and the polymer. Injections of a modified silicate during the polymerization (in situ method[11,12]) to a solvent-swollen polymer (solution blending[13]) or to the polymer melt (melt blending[14]) are examples of molecular-level control. With this kind of intercalation polymerization, we could systematically examine the polymer conformation in a confined, nanometer-sized inorganic gallery.

Layered smectite-type montmorillonite (MMT), a hydrous alumina silicate mineral whose lamellae consists of octahedral alumina sheets sandwiched between two tetrahedral silicate sheets, exhibits a net negative charge on the lamellar surface. This structure enables the surface to adsorb cations, such as Na^+ or Ca^{2+}. Compatibility with various polymers is accomplished by modifying the silicates surface with organic cations via an ion exchange reaction.[14] The cationic headgroup of the alkylammonium molecule preferentially resides at the layer surface, while the aliphatic tail is away from the surface. The presence of these aliphatic chains in the galleries modifies the original hydrophilic silicate surface to be organophilic. Additionally, the organic cations may contain various functional groups, which can react with the polymers and improve adhesion between the reinforcement particles and the matrix. Thus, it is possible to obtain nanocomposites with good dispersion quality in organic solvents and to increase the spacing between the clay layers by increasing the surfactant chain length and the charge density of the clay.[15]

Recently, nanocomposite composed of poly(ethylene oxide) (PEO) intercalated between the layers of mica type clay showed possibilities as a new class of polymer composite electrolytes.[16−19] In the case of nanocomposite, PEO forms the matrix for a solid-state electrolyte whose conductivity is primarily cationic, because the anions are the large clay layers. The effect of layer charge on the intercalation of PEO is also investigated using a series of reduced MMT and smectites with varying layer charge.[19] A computer simulation is performed to examine the atomic scale structure and dynamics of intercalated PEO/MMT nanocomposite.[20] Even though the structure and thermal/mechanical properties of PEO/clay nanocomposites were extensively studied, there are limited studies on the rheological behavior of PEO/clay nanocomposite.

In polymer processing, such as injection molding and extrusion, the mechanical/rheological properties of these

† Inha University.
‡ Carnegie Mellon University.
* Corresponding author. E-mail: hjchoi@inha.ac.kr.

10.1021/ma002191w CCC: $20.00
Published on Web 10/12/2001

nanocomposites, which are related to the microstructure, the state of the dispersion, the shape and orientation of the dispersed particles, and particle−particle interactions, are of vital importance. Especially, the state of the dispersion can be studied at two levels: (i) the macroscopic level, which involves the measurements of the rheological properties of the bulk blend, or (ii) the microscopic level, which investigates the detail dynamics of the individual particles.[21] The mesoscopic structure is critically dependent not only on the strength of the polymer/clay interaction but also on the inherent viscoelastic properties of the matrix in which the layers (or collection of layers) are dispersed.[22] Lim and Park,[23] in their quantitative analysis, reported that the rheological behavior of intercalated polystyrene (PS)/layered silicate nanocomposites are correlated to the microstructures of the nanocomposites and that the microstructural changes cause temporal behavior. The rheological behavior of polymer/clay nanocomposite depends not only on their microstructure[24] but also on their interfacial characteristics.[25] Krishnamoorti et al.[26] examined the rheology of end-tethered polymer, layered silicate nanocomposites prepared by in-situ polymerization, consisting of poly(ϵ-caprolactone) (PCL) and nylon-6 with various amounts of layered silicate. They used a lattice model for the interactions between polymers and organoclays which showed that the conformation of the polymers and surfactants are decoupled.[27,28] Thus, the configurations of the free and tethered species are independent of each other. Furthermore, the intercalated hybrids offer a unique avenue to study the static/dynamic behavior of macromolecules confined in nanoscale.

In our study, different organoclay series and PEO were intercalated via a solvent casting method using chloroform as a solvent,[18] compared to melt intercalation of PEO/clay.[17,19] Nanocomposites prepared by dispersion of organoclay in small molecular organic solvent are one of many nanocomposite preparation methods. The solvent casting methods[29,30] have also been adopted to produce poly(L-lactide) (PLLA)/MMT and PCL/MMT intercalated nanocomposites. To investigate both the dispersion of the organoclay and interaction between the surfactant and polymer, we used three types of surfactants. First, we selected two different organclays, which have different modifier concentration (MC) but the same alkylamonium salts. Second, we differentiated the types of alkylamonium salts having the same MC. Furthermore, the effect of clay content on PEO/organoclay nanocomposites has been investigated. Rheological studies of these systems showed that there is a dramatic alternation in structure by the imposition of steady and small-amplitude oscillatory shear.

Experimental Section

Materials and Preparation. Three organoclays (Cloisite 15A, 20A, and 25A or CX, CY, and CZ, respectively) were obtained from Southern Clay Products (Gonzales, TX). Cloisites are produced by an ion exchange reaction, where the quaternary ammonium cations replace the sodium cations on an MMT clay surface. Cationic exchange capacity (CEC) was 95 mequiv/100 g for all MMT used in the Cloisite series,[31] in which the CEC is a property of a layered silicate derived from isomorphous substitution in a crystal lattice. Usually, isomorphous substitution occurs when, during the formation of the clay, an element replaces silicon or aluminum in the clay structure. For the substitution to obtain a stable clay, the substituting element must be the same size as silicon or aluminum. The most common substitution is aluminum for silicon in the tetrahedral sheets and magnesium for aluminum in the octahedral sheet. Substitution is common in the clays having "2:1" structure, but not in "1:1" type. Isomorphous substitution is one of the sources of a clay CEC.

Table 1. Organoclay Series Modified with Surfactants

sample codes	organoclay (commercial name)	modifier concn (mequiv/100 g)	d_p (Å)	d (Å)	$\Delta d \equiv d - d_p$ (Å)
CX	Cloisite 15A	125	32.2	37.4	5.2
CY	Cloisite 20A	95	24.7	36.7	12.0
CZ	Cloisite 25A	95	21.8	32.1	10.3

On the other hand, the amount of surfactant added to the MMT in the exchange reaction is referred to as the MC and also noted in mequiv/100 g of MMT in Table 1. Two different surfactants of dimethyl hydrogenated tallow 2-ethylhexyl quaternary ammonium (CZ) and dimethyl dihydrogenated tallow quaternary ammonium (CX and CY) have been treated. It has been known that pure organoclay interlayers spacing becomes higher with both surfactant chain length and the MC of the clay surface, because both of these parameters contribute to the increase in volume occupied by the surfactant.[15] The d spacings of pure organoclay (d_p) and those after PEO insertion (d) were measured by X-ray diffraction (XRD), as shown in Table 1.

The matrix PEO (M_W = 200 000 g/mol) was purchased from Scientific Polymer Products Inc. (Ontario, NY). PEO is a linear, nonionic polymer that can be used as a solid solvent for metallic salts.[32] PEO can also be used for an electrolyte material in solid-state batteries, sensors, etc. To improve the electrochemical performance of the polymer electrolytes, inorganic fillers, such as MMT, have been added.[17,33,34] The intercalation method via either insertion of a suitable monomer and subsequent polymerization or direct insertion of polymer chains from the solution or the melt has been used. This depends on the strength between the layered clay and the polymeric species. In contrast to intercalated hybrids, the host of exfoliated nanocomposite layers is dispersed in a continuous polymer matrix. The interlayer expansion in exfoliated hybrids is on the order of the radius of gyration of the polymer without their structural registry.[35]

Both organoclay and PEO were dried in a vacuum to remove moisture. We used the three different organoclays with the same composition to compare the effect of clay property on the rheological properties. 10 g of PEO was dissolved in chloroform, and 1 g of organoclays (powder form) was dispersed in 200 mL of chloroform for 2 days. To promote the swelling and expansion of the layer spacing, only organoclay dispersed in chloroform was sonicated for 1 h using an ultrasonic generator (Kyung-ill Ultrasonic Co., Korea) at a frequency of 28 kHz. These sonicated organoclay dispersions and nonsonicated PEO solutions were then mixed together while stirring for 2 days, and the mixtures were placed in glass dishes. After the chloroform was evaporated in a hood, all of the samples were subsequently dried in a vacuum oven for 1 day. The weight percent of the organoclay in PEO/organoclay nanocomposites was fixed at 9 wt %.

To investigate the clay volume effect on the nanocomposite, different amounts of CZ and PEO [CZ/(CZ + PEO) × 100 = 2, 5, 9, and 17 wt %] were dispersed/dissolved in chloroform. Finally, the film-type PEO/organoclay nanocomposites were made with a compressed mold (Carver, model 3852, USA) at 120 °C.

X-ray Diffraction (XRD). The insertion of PEO into the organoclay layers was confirmed by XRD. A Guinier focusing camera, using a quartz crystal monochromator in a Philips PW-1847 X-ray crystallographic unit (40 kV and 40 mA) fitted with a copper target, was used for recording data in the range of $2\theta = 1.5°-10°$ for PEO/organoclay nanocomposites at given organoclay content and also in the range of $2\theta = 1.5°-35°$ for PEO/CZ nanocomposite with various CZ loading.

Transmission Electron Microscopy (TEM). TEM photographs were obtained with a JEM 2000 EX-II(JEOL, Tokyo, Japan) electron microscope operated at an accelerated voltage

of 100 kV. All of the ultrathin sections (less than 3 μm) were microtomined using Super NOVA 655001 (R. J., Swiss) with a diamond knife and then subjected to TEM observation without staining.

Rheological Properties. The rheological properties are related to the distortion or deformation of the nanocomposites. Despite of its importance, the dependences of rheological properties on the intercalated/exfoliated structures, and the surface characteristics between the polymer chains and clays have not been thoroughly investigated. We used a Physica MC120 rotational rheometer (Stuttgart, Germany) with a parallel plate geometry, using 25 mm diameter plates at a fixed temperature of 120 °C. Note that the melting temperature (T_m) of PEO from DSC measurement is 66 °C. Shear viscosities were measured as a function of shear rates for the molten state of the sample. The oscillatory measurements were also performed to study the durability of the nanocomposites in the presence of vibration or external stress. During the measurement we set the amplitude to be 0.03 to ensure the linear viscoelastic region. G' represents the strain energy reversibly stored in the substance, while G'' represents the amount of energy irreversibly given off by the substance to its environment.

In the linear viscoelastic regime with small sinusoidal strain ($\gamma(t) = \gamma_0 \sin(\omega t)$), the stress $\tau(t)$ is represented by

$$\tau(t) = \gamma_0[G'(\omega)\sin(\omega t) + G''(\omega)\cos(\omega t)] \quad (1)$$

Here, γ_0 is the strain amplitude, ω is the frequency, and t is real time. $\tan\delta = G''/G'$ indicates the ratio between the amount of the dissipated and the stored energy, i.e., the ratio between the viscous and the elastic response of the sample. $\tan\delta$ becomes very large ($\gg 1$) for liquidlike materials, while it becomes very small ($\ll 1$) for solidlike materials. The magnitude of complex viscosity is given by

$$|\eta^*| = \sqrt{(\eta')^2 + (\eta'')^2} \quad (2)$$

η' is the real part of the complex viscosity, which stands for the viscous behavior, while η'' is the imaginary part of the complex viscosity, which stands for the elastic behavior.

Thermal Properties. The thermal properties were measured via a thermogravimetric analysis (TGA) (Polymer Lab., TGA1000, UK) from 20 to 470 °C, under a nitrogen atmosphere at a heating rate of 20 °C/min, and a differential scanning calorimeter (DSC) (Perkin-Elmer, series 7) at a heating rate of 10 °C/min. T_m and the latent heat of fusion (ΔH_m) were obtained from the maximum endothermic peak position and area of the DSC curves.

Results and Discussion

Figure 1a shows the XRD patterns of the PEO nanocomposites with various types and concentrations of organoclay. The different d_p values in the three pure clays are attributed to the respective size of the surfactant and MC of the surface. The intercalation of the polymer chains usually increases with the interlayer spacing of the clays, in comparison with interlayer spacing of the pure clays, leading to a shift of the diffraction peak toward lower values of θ. XRD parameters are summarized in Table 1, where the d_p and d were calculated using the Bragg formula ($\lambda = 2d \sin\theta$). The XRD pattern reveals a diffraction peak for PEO/CX9 that has been shifted toward a higher interlayer spacing than those of PEO/CY9 and PEO/CZ9. From XRD, we observed that the larger surfactant size and higher concentration on the clay surface result in a smaller interlayer spacing difference of the clays ($\Delta d \equiv d - d_p$). It can be thought that regardless of the initial MC and the orientation of the long chain surfactants, the gallery height is determined by the vertical orientation of the long chain surfactant in the intercalation.[15] The lower expandability of high-charge smectites and vermiculites in organic solvents such as glycol and glycerol[36] was also considered originating from the higher attractive electrostatic forces, the high density of hydrated exchangeable cations, and the lack of accessible surfaces for adsorption.[19] From these results, they also contain multiple, ordered platelets.[28] Accordingly, it can be conjectured that dispersion of clay in the polymer matrix is related to platelets agglomerated into clay particles, not to individual clay platelets. Figure 1b illustrates XRD patterns of the CZ-based nanocomposites with clay loading. The d of the CZ in the polymer matrix increased with CZ loading; d spacing increased from an original value of 2.18 nm to 3.12 and 3.52 nm for PEO/CZ2 (magnification is shown in Figure 1b) and PEO/CZ5, ruling out the contribution by the intensity increase from the PEO crystal for PEO/CZ with 2 wt % of CZ. Note that the pure PEO also shows low-angle scattering due to its crystal lamella scattering of the crystalline regions and the intensity of XRD peaks corresponding to the pure PEO is progressively reduced with the CZ loading. However, when the amount of CZ increases beyond 5 wt %, no significant increase in

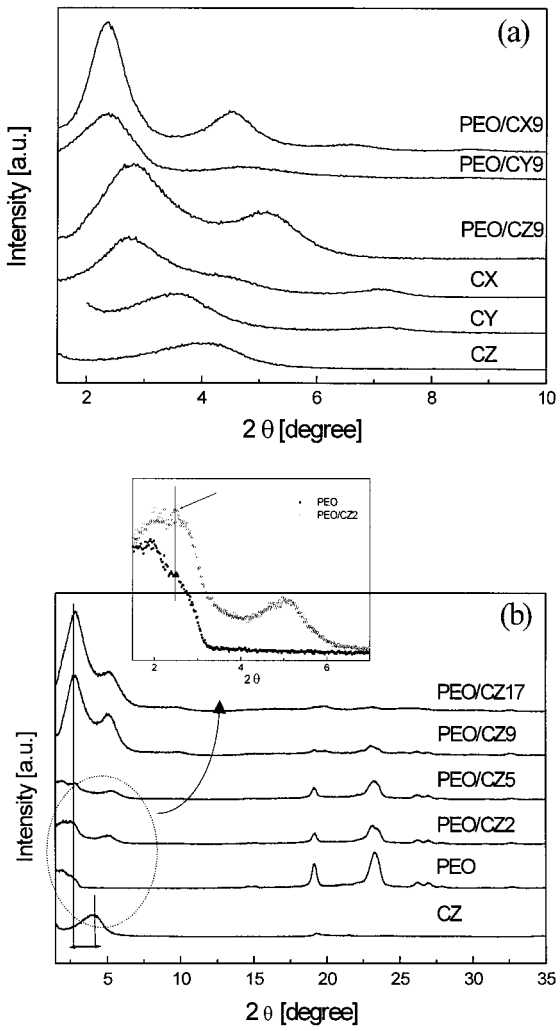

Figure 1. XRD patterns for (a) various PEO/organoclay nanocomposites (9 wt %) and pure organoclays and (b) PEO/CZ with various CZ loading. Data in the range of $2\theta = 1.5°-10°$ for PEO/organoclay nanocomposites with fixed organoclay content and also in the range of $2\theta = 1.5°-35°$ for PEO/CZ nanocomposite with various CZ loadings.

gallery height (3.21 and 3.12 nm for PEO/CZ9 and PEO/CZ17, respectively) was observed. We also observed that the intensity of the XRD peaks becomes smaller with CZ loading.

The internal structures of the nanocomposites in the nanometer scale were observed via a TEM. The structure of nanocomposites has typically been elucidated using TEM and wide-angle X-ray diffraction (WAXD). TEM allows a qualitative understanding of the microstructure through direct visualization. On the other hand, WAXD offers a convenient method to determine the interlayer spacing due to the periodic arrangement of clay layers in the original clay and in the intercalated polymer/clay nanocomposites. However, WAXD does not provide definitive structural information for the exfoliated or delaminated state where the periodic arrangement is lost. WAXD also has drawbacks of weak peak intensity, bias toward surface region, and poor peak resolution, particularly for the composites with small clay content.[37] The subtle changes in the mesoscopic structure could be poorly characterized by WAXD, yet will yield a large rheological effect.[21] Figure 2 shows the TEM images of the nanocomposites: (a) PEO/CX9 (×10 000), (b) PEO/CY9 (×10 000), (c) PEO/CZ9 (×10 000), and (d) PEO/CZ9 (×50 000), in which the dark entities are intercalated organclay layers. It is clear that stacks of organoclay layers forming the clay crystallites are dispersed within the polymer matrix. For better understanding of intercalated tactoid structure, we magnified the PEO/CZ9 case (Figure 2d). In this figure, we can find the well-ordered tactoid structure (multilayer particles) of polymer/clay nanocomposites.

In the rheological characterization of the nanocomposite, the steady shear response of clay-based polymer nanocomposite will provide useful information on the material processability. There exist several studies for the rheological behavior of polymer/clay nanocomposites with weak adsorbing parts.[38,39] We have examined the PEO/clay intercalated nanocomposites. The steady shear viscosity, η, as a function of shear rate, $\dot{\gamma}$, for several nanocomposites is shown in Figure 3a,b.

Figure 3a shows the measured η of PEO, PEO/CX9, PEO/CY9, and PEO/CZ9 nanocomposites. The viscosities of nanocomposites are much higher than that of pure PEO. The η of the PEO/CX9 is higher than that of PEO/CY9, since their MC are different (see Table 1). Considering the size of surfactant, the shear viscosity of PEO/CY9 is larger than that of PEO/CZ9, because of the difference in initial spacing of pure organoclays. These enhancement arises from the interaction and dispersion of clay in the polymer matrix. Although the η of PEO/CX9 is larger than that of the others, all of these nanocomposites have similar η at high shear rates due to the alignment and orientation of clay particles. (They aligned differently at the same shear rate since λ is different.) According to these results, the clay particles in PEO/CX9 are better dispersed in PEO matrix than PEO/CY9 and PEO/CZ9. Therefore, it can be conjectured that dispersion of clay particles is related not only to individual clay platelets but also to clay platelet agglomerate, (e.g., like dispersed intercalated tactoids). Ren et al.[40] suggested that the mesoscopic structure consists of clay tactoids of several tens of well-ordered layers and the occasional presence of individual layers removed from the tactoids for the polystyrene−polyisoprene block-copolymer-based intercalated nanocomposites. Therefore, different surfactants adsorbed to the exterior surface of the multiplatelet domains mediate differences in the attractive interparticle interactions that give rise to the nanocomposite structure. Alternatively, the size and shape of the multiplatelet domains could depend on surfactant chemistry. Figure 3b shows the η for various PEO/CZ nanocomposites with several CZ loadings. The η increased substantially at low shear rates with CZ loading. As shear rate increases, these nanocomposites display more drastic shear-thinning behavior with CZ loading. A similar trend has been observed by Krishnamoorti et al.[35] for a series of intercalated poly(dimethyldiphenylsiloxane)/layered silicate (dimethyl ditallow MMT) nanocompsoites with several different silicate loadings. They observed that the shear viscosity of the nanocomposites increased monotonically with clay loading, and the intercalated nanocomposites display a shear thinning behavior at low shear rates (even though viscosity of the pure poly(dimethyldiphenylsiloxane) is shear rate independent). In other words, at low shear rates, the addition of very small amounts of clay results in non-Newtonian behavior as well as a significant enhancement in the shear viscosity. However, at high shear rates, the shear viscosity and shear thinning behavior for the nanocomposites are comparable with those of the pure polymer as a result of the preferential orientation of the clay layers or even anisotropic tactoids parallel to the flow direction.

To investigate the dependence of the η on $\dot{\gamma}$, we employed the Carreau model,[41] which has proven to be a useful model for fitting the non-Newtonian viscosity curve for various polymeric systems:[42,43]

$$\eta = \frac{\eta_0}{[1 + (\dot{\gamma} t_1)^2]^{(1-n)/2}} \tag{3}$$

Here, η_0 is the zero shear rate viscosity, t_1 is the characteristic time, and n is a dimensionless parameter. The slope of η vs $\dot{\gamma}$ on a log−log plot in the power-law region is $(n - 1)$. For $n = 1$ or $\dot{\gamma} t_1 \rightarrow 0$, eq 3 reduces to the Newtonian fluid behavior, and this model predicts shear-thinning behavior for $n < 1$. The calculated values of η_0, t_1, and $(1 - n)$ (Table 2) increased with CZ content. Furthermore, we observed $(1 - n)$ and η_0 increase drastically for 17 wt % content and exhibit a sharp transition from the Newtonian plateau region to the power-law region. These frictional interactions between the anisotropic clay can become significant with higher clay content, which results in a strong dependence of the viscosity on clay loading.[37] In addition, we found that there exists a critical shear rate ($\dot{\gamma}_c$), which is defined as the onset point of shear-thinning transition (Figure 3b). $\dot{\gamma}_c$ is approximately equal to the inverse of t_1 (or the longest relaxation time[44]). From Table 2, $\dot{\gamma}_c$ is estimated as 0.228, 0.060, 0.050, 0.040, and 0.035 s^{-1} for PEO, PEO/CZ2, PEO/CZ5, PEO/CZ9, and PEO/CZ17, respectively. The location of $\dot{\gamma}_c$ is plotted in Figure 3b. Also, the addition of clay has a profound effect on the terminal relaxation time of the nanocomposites. With increasing clay loading, the liquidlike relaxation observed for the pure polymer gradually changes to solidlike (or pseudo-solidlike) behavior for nanocomposites.[40] The criteria for liquidlike to solidlike transitions of the polymer melt are also obtained via $G'(\omega)$, $G''(\omega)$, and $\eta(\dot{\gamma})$ measurements.[44] The transition from a liquidlike to solidlike state has been observed in other systems (including the noncolloidal suspensions of hard spheres[45] and electrorheological suspensions[46]).

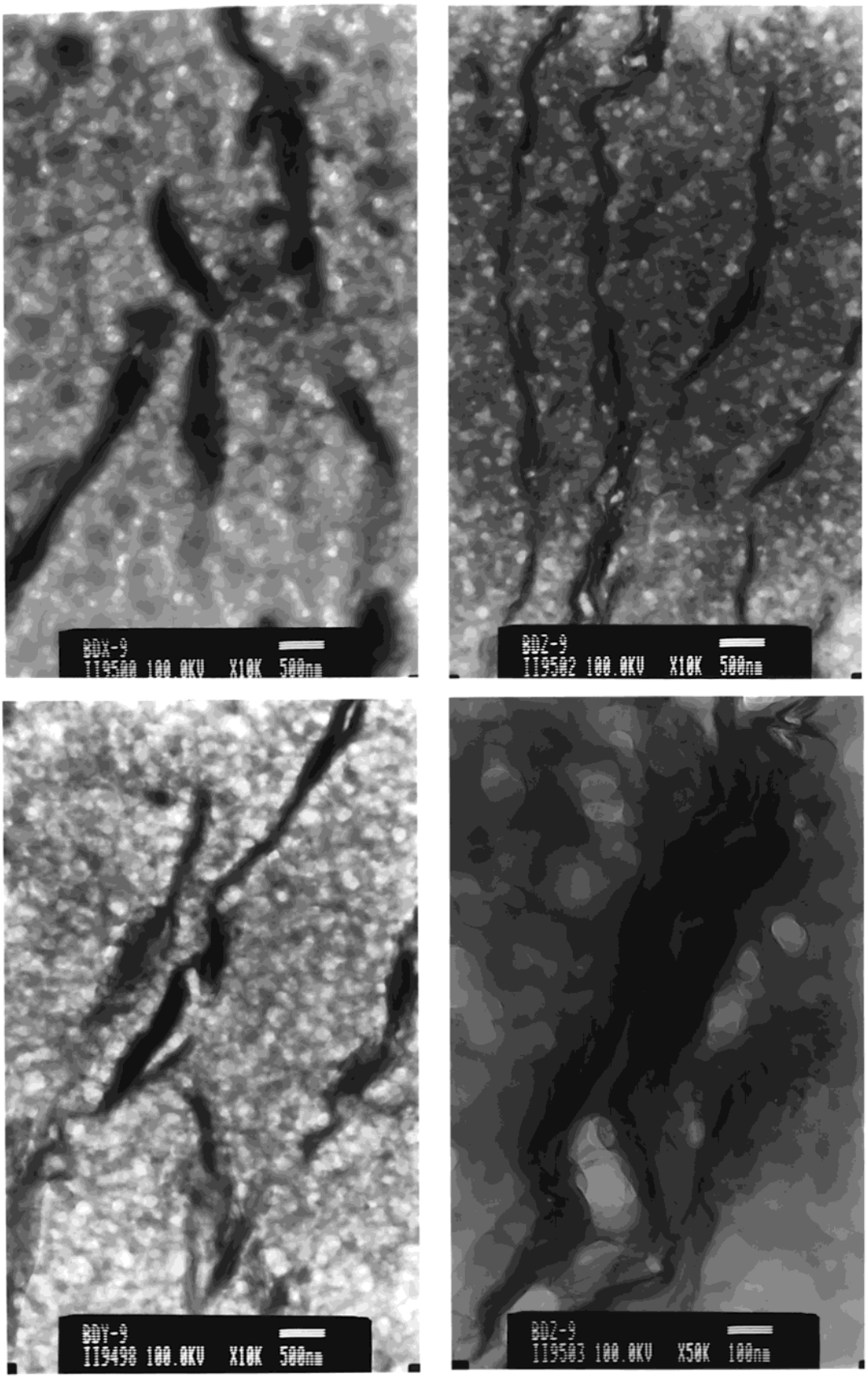

Figure 2. TEM of various PEO/organoclay nanocomposites (9 wt %): (a) PEO/CX9 (×10 000, 500 nm), (b) PEO/CY9 (×10 000, 500 nm), (c) PEO/CZ9 (×10 000, 500 nm), and (d) PEO/CZ9 (×50 000, 100 nm).

As illustrated in Figure 3, the flow curves of the nanocomposites possess two distinct regions: a Newtonian region and a power law (shear-thinning) region. The Newtonian region is observed at very low shear rates, where the η is independent of $\dot{\gamma}$. In the power-law region, the viscosity decreases linearly with increasing shear rates on log−log plots. Figure 4a,b shows the normalized shear viscosity as a function of shear rate.

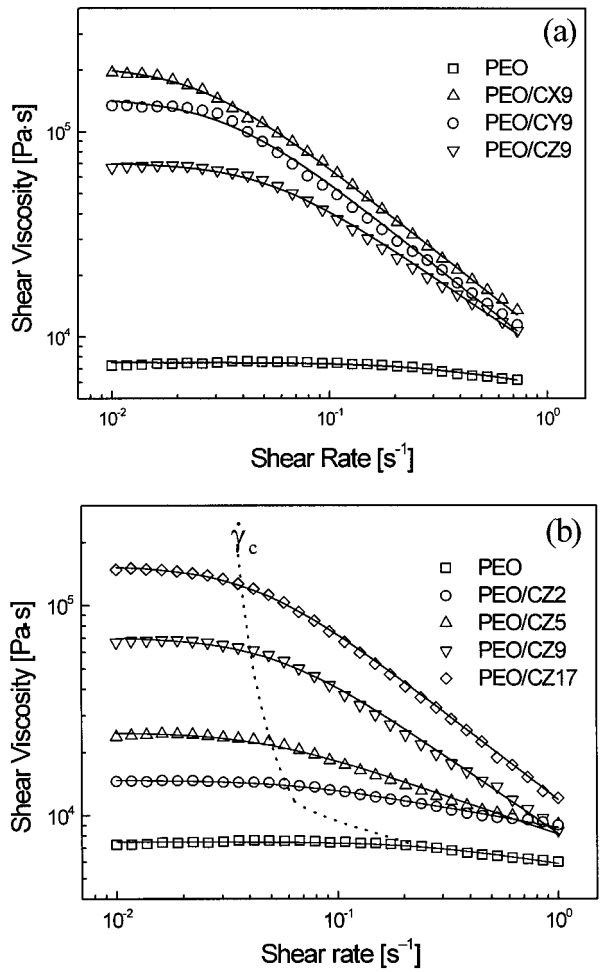

Figure 3. Shear viscosity vs shear rate (a) for various PEO/organoclay (9 wt %) nanocomposites and (b) for PEO/CZ nanocomposites with several CZ loadings. Symbols are the experimental data, and solid lines are the best fits with eq 3.

Table 2. Parameters in Carreau Model [Eq 3] for PEO and Various Nanocomposites

sample code	η_0 (Pa s) × 10^{-4}	t_1(s)	n
PEO	0.75	4.37	0.84
PEO/CX9	21.0	39.22	0.17
PEO/CY9	14.40	29.60	0.15
PEO/CZ9	7.0	21.88	0.27
PEO/CZ2	1.48	16.11	0.81
PEO/CZ5	2.50	18.86	0.64
PEO/CZ17	15.60	23.45	0.19

Although the zero shear rate viscosity of PEO/CX9 is higher than that of PEO/CY9, n of PEO/CY9 is smaller than that of PEO/CX9. In addition, we found that n decreased with CZ content, and $\dot{\gamma}_c$ decreases with CZ loading. These curves clearly demonstrate a Newtonian region at low shear rates and a well-defined power-law region at higher shear rates.[47] Furthermore, n of these nanocomposites became significantly smaller than that of PEO.[48] Although the mechanism of shear-thinning behavior for nanocomposites is not fully understood, we speculate that it might be due to the orientation of silicate layers and polymer conformation changes under shear. With increasing shear rate, the conformations of the intercalated chains are also expected to change as silicate layers align parallel to the flow field.[49,50] Also, the mesoscopic structures of multiple, ordered platelets which are the dominant structure for nonlinear deformation are due to the aniostropic structure of clay.

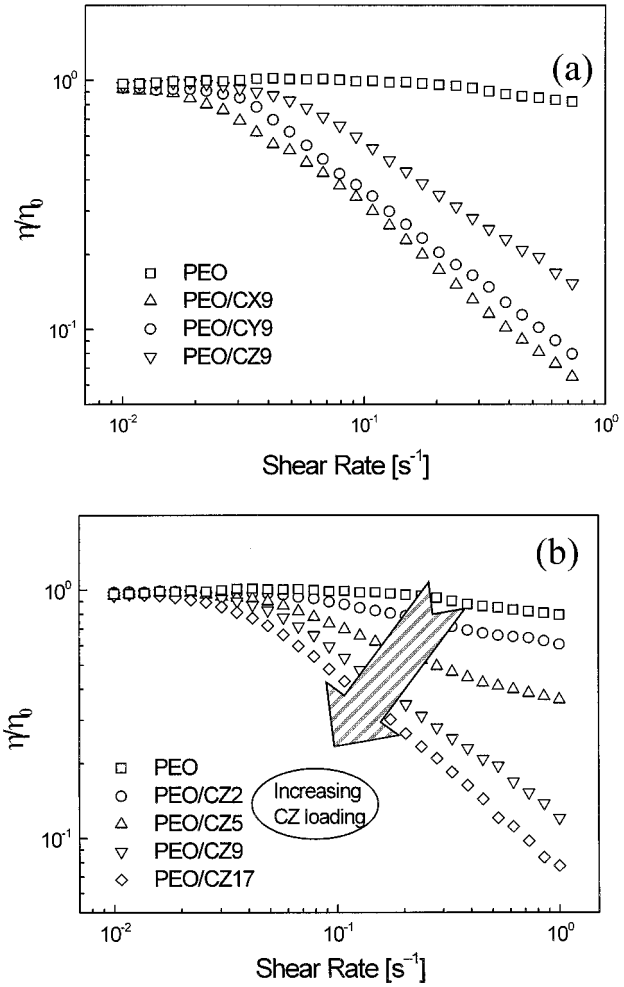

Figure 4. Normalized shear viscosity η/η_0 of (a) various PEO/organoclay (9 wt %) nanocomposites and (b) PEO/CZ nanocomposites with several different CZ loadings. η_0 is obtained from eq 3.

A hysteresis in the flow curve was also observed in a complete cycle of the shear rate measurement and was plotted in Figure 5. In the hysteresis loop experiment, the shear rate is increased from 0.01 to 1 s^{-1}, held for 1000 s, and then linearly decreased from 1 to 0.01 s^{-1}. As given in Figure 5, a hysteresis phenomenon is observed for all our nanocomposite samples except for pure PEO. The hysteresis loop areas, which are the area enclosed by the increasing and decreasing loops, increase with clay content. For the decreasing shear rate process, partial recovery of the viscous structure took place when the cycle was over. The viscosity of the material has nearly recovered to the shear viscosity of pure PEO because the shear rate of 1 s^{-1} was close to $\dot{\gamma}_c$. This value is very different from the nanocomposites with different clay loading (PEO/CZ5, CZ9, and CZ17). In other words, the rate of destruction of viscous properties after shear is initially applied is larger than the rate of recovery after shear is reduced. The structure of nanocomposites might not reach an equilibrium state or the initial structure after the completion of the hysteresis experiment. Since the entanglement of the polymer chain and arrangement of clay is not permanent and is altered by flow and relaxation processes, any disturbance such as shear will disrupt the structure of polymer matrix in the presence of clay particles.

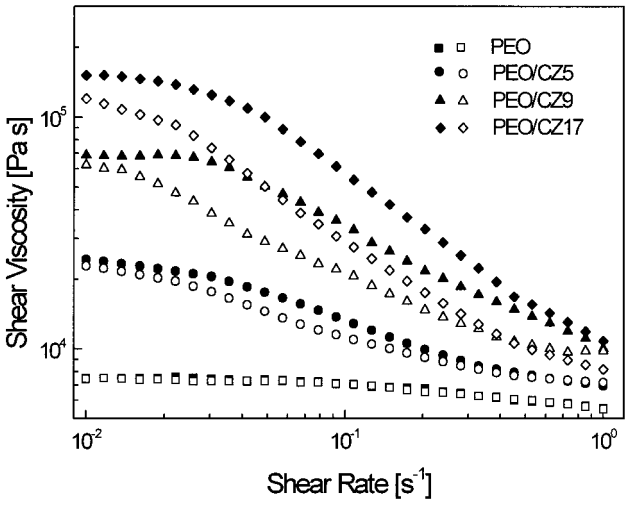

Figure 5. Hysteresis loops for PEO/CZ nanocomposites with three different clay contents. Filled symbols represent measurement under increasing shear rates, and open symbols represent decreasing shear rates experiment for cyclic process of 1000 s.

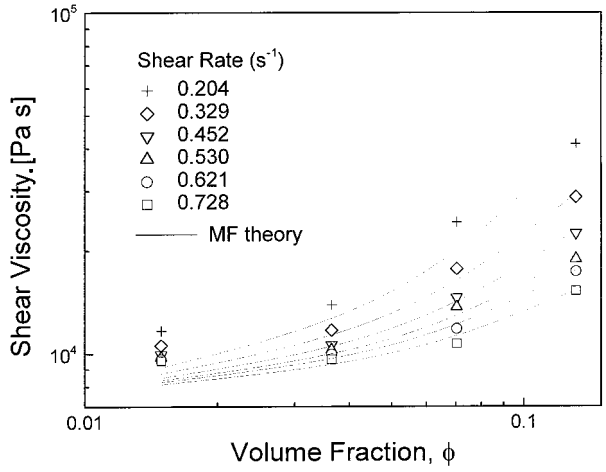

Figure 6. Shear viscosity vs volume fraction. Symbols are the experimental data. Solid lines are fits using the MF equation (eq 4b).

We have adopted mean-field (MF) theory to examine this behavior. It is well-known that the viscosity of suspension is represented by a Taylor expansion in the volume fraction, ϕ, for dilute concentration. However, this series become difficult to implement as concentration increases.

In MF theory,[51] the incremental viscosity changes by the addition of dϕ into the suspension of viscosity; $\eta(\phi)$ becomes

$$\eta(\phi + \mathrm{d}\phi) = \eta(\phi)[1 + \mathrm{d}(\ln \phi)] \qquad (4a)$$

Assuming that $\eta(\phi)$ obeys Einstein's theory of intrinsic viscosity $[\eta]$, and by solving eq 4a, we obtain

$$\eta = \eta(\phi = 0)(1 - \phi/\phi_\infty)^{-[\eta]\phi_\infty} \qquad (4b)$$

Here $\eta(\phi = 0)$ is the viscosity of the suspending medium. ϕ_∞ represents the concentration at which particles are packed such that the viscosity of the suspension becomes infinite.

Figure 6 shows the plots of viscosity as a function of the CZ volume fraction. The MF equation describes the viscosity data very well except in the low shear rate and low concentration regions.

The dynamic oscillatory measurement is used to analyze the mesostructure and should be kept within the linear viscoelastic region so as not to destroy the structure of the sample; very high stresses prevent the sample from remembering its initial state after relief. The linear viscoelastic range must be within a limited range of amplitude and oscillation frequency (e.g., by an amplitude sweep test). Thus, we chose strain to be 0.03.

For the small-amplitude oscillatory shear studies in PEO/CZ nanocomposite systems, a linear rheological response was observed only for a limited range of strain. Comparison of the linear viscoelastic response for the five different PEO/CZ systems indicates the significant effect of clay loading.

G' and G'' are measured for nanocomposites with different clay content by dynamic oscillatory measurements (Figure 7a,b). G's of these nanocomposites exhibit a monotonic increase for all frequencies. The transition of G'' from the sharp slope and terminal linear viscoelastic behavior are observed for low CZ content (2 and 5 wt %), including pure PEO. However, nonterminal linear viscoelastic behavior was observed for clay contents larger than 9 wt %. Namely, the low-frequency response is indicative of a solidlike behavior except 9 wt % clay. Solidlike behavior has been observed in conventional, filled polymer systems in which there exist strong interactions among the polymers and the fillers.[52] Thus, the presence of the clay layers and the lack of complete relaxation of the chains contribute to the solidlike response at low frequencies. Larson[44] also demonstrated the storage and loss modulus for liquidlike and solidlike materials. For the liquidlike behavior, the G' is much lower than the G'', and vice versa for the solidlike system. At low frequencies, the PEO melt behavior is liquidlike ($G' < G''$), while inheriting solidlike behavior at high frequencies ($G' > G''$). In that case, the transition of pure PEO from liquid to solidlike behavior occurs at crossover frequency (ω_c) of approximately 93 1/s. The ω_c for these nanocomposites was shifted toward a lower frequency with increasing clay content (ω_c is ~36 1/s for 5 wt % system). However, the nanocomposites over 9 wt % did not possess ω_c because $G' > G''$ at low frequency. On the basis of mesoscopic structure at low clay concentrations, it is suggested that, beyond a critical volume fraction, the tactoids and individual layers are incapable of rotating freely and are prevented from complete relaxation when subjected to shear. This incomplete relaxation due to the physical jamming or percolation lead to the presence of the pseudo-solidlike behavior observed in both intercalated and exfoliated nanocomposites.[40] Thus, it appears that intimate contact between the polymer and the clay platelets alters the relaxation processes of the polymer, leading to the low-frequency plateau in the shear moduli and non-Newtonian viscosity behavior with clay loading at the low-shear rate.[26] There exist more pronounced interactions between the clay platelets and higher tendency to form a three-dimensional superstructure. The end-tethered polymer chains on the clay layers stabilize this superstructure.[53] It can be also noted that Pignon et al.[54] studied the characteristic length scale of the network structure of a colloidal suspension of synthetic clay and found that changes in fractal dimensions govern the elastic modulus.

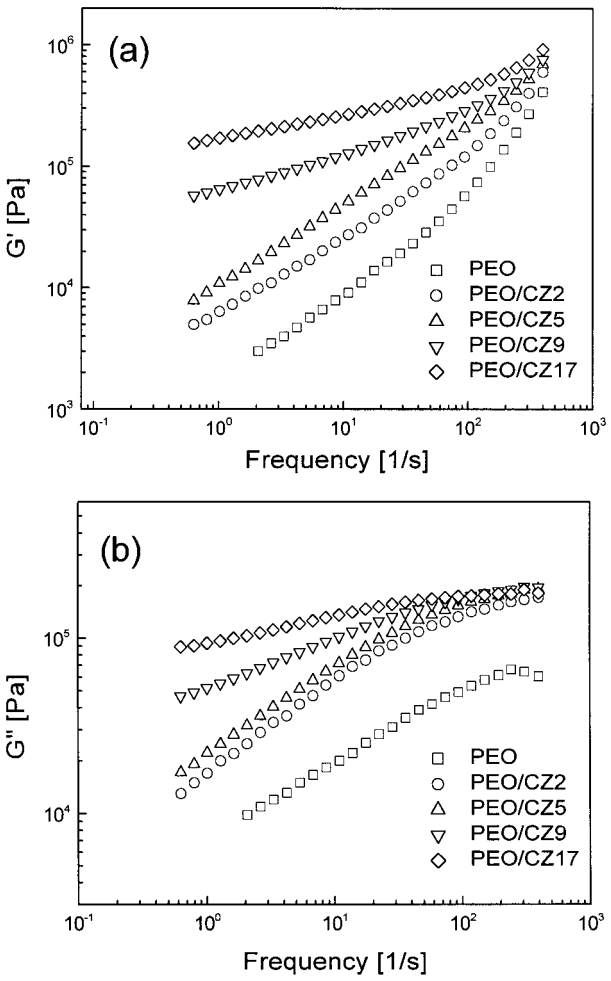

Figure 7. (a) G' and (b) G'' for PEO/CZ nanocomposites for several different CZ loadings.

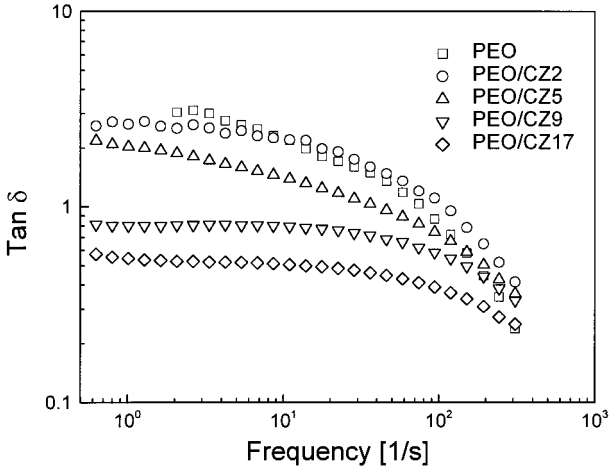

Figure 8. tan δ vs frequency for PEO/CZ nanocomposites with several different CZ loadings.

Figure 8 shows the frequency dependence of tan $\delta = G''/G'$ for nonassociated (tan $\delta > 3$), weakly associated ($1 <$ tan $\delta < 3$), and strongly associated (tan $\delta < 1$) dispersed particles.[55] tan δ also is dependent on clay content. For low CZ content (PEO/CZ2 and PEO/CZ5), tan δ is greater than 1, while tan δ becomes smaller than 1 for high CZ content (PEO/CZ9 and PEO/CZ17). To separate the two effects (clay content and interaction), we have plotted the absolute value of the η^* against the tan δ. Here, tan δ was obtained from two distinct regions: 0.628−6.28 and 6.28−62.8 1/s. In other words, we calculated two average tan δ values for each system in a different region. The tan δ was an averaged value. If the clay platelet interactions change only as a result of separation distance, all the data will collapse onto a single line. However, for the nanocomposites with different clay platelet interactions, the data did not collapse onto a single line. Thus, it shows that the clay structure is forming tactoid consisting of clay platelets. This relationship is shown in Figure 9.

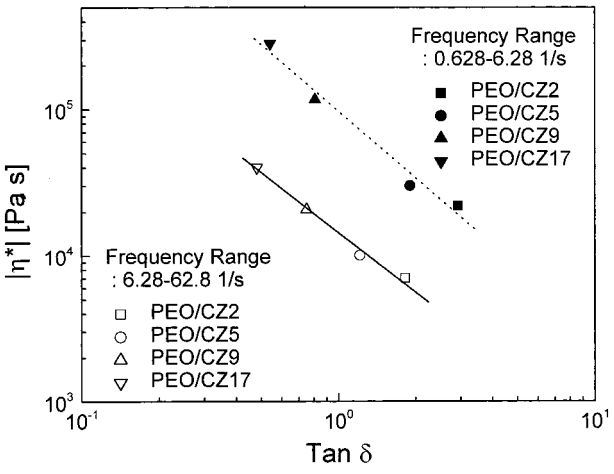

Figure 9. Maximum $|\eta^*|$ vs averaged tan δ obtained from two distinct frequencies region.

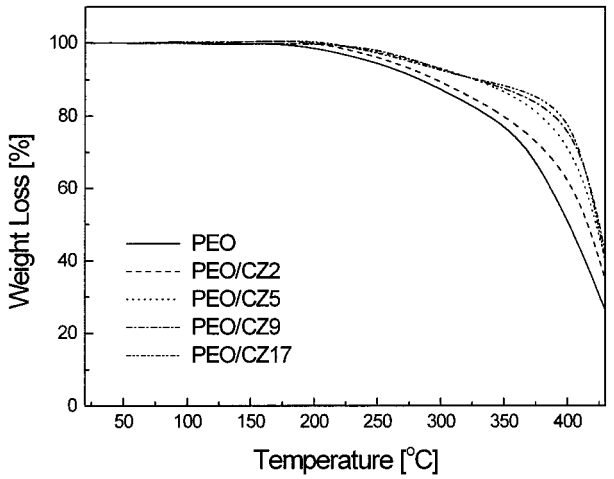

Figure 10. TGA curves for pure PEO and PEO/CZ nanocomposites with several different clay loadings.

An increase of thermal stability has also been observed for intercalated nanocomposites (Figure 10). The nanocomposites degrade at substantially higher temperatures than pure PEO. It is clear that a large increase in the onset of decomposition occurs for nanocomposites with high CZ content, except for PEO/CZ9 and PEO/CZ17. Near 200 °C, it is hypothesized that intercalated organic matter (surfactant) starts to be lost in one or two steps, respectively. It is known that silicate has a good barrier property against permeation of various atmospheric gases. The addition of clay enhanced the performance of the char formed, by acting as a superior insulator and mass transport barrier to the volatile products generated during decomposition.

As shown in Figure 11, T_m and ΔH_m decrease with increasing CZ content, implying that small-sized PEO

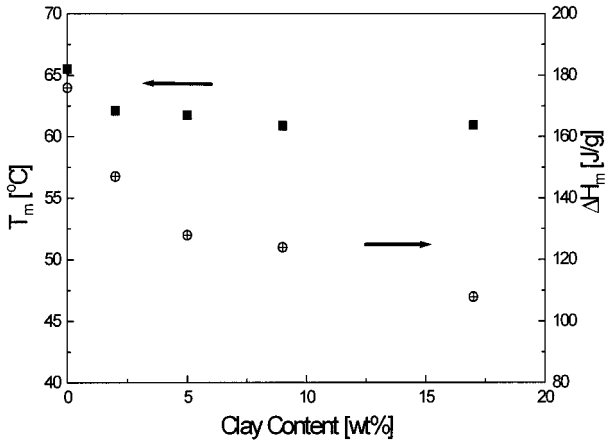

Figure 11. Effect of CZ content on T_m and ΔH_m.

crystallites are formed in the presence of the clay. The decrease in T_m of PEO indicates that intercalation of PEO leads to a confinement of the chain that prevents polymer crystallinity.[18] The ΔH_m decrease with clay content indicates that the total crystallinity of PEO is influenced by the presence of the CZ. Recently, Vaia et al.[56] compared T_m of PEO/nanocomposite obtained from the melt and solution intercalation based on water. The solution intercalation contained a fraction of unintercalated PEO chains which exhibits a weak and depressed PEO melting endotherm. In contrast, the melt intercalation was starved, such that almost all of the PEO chains were effectively intercalated.

Concluding Remarks

In solvent cast nanocomposites, the intercalation of PEO chains between interlayers of organoclay was examined by XRD. Although the larger surfactant size and higher concentration on the clay surface result in a smaller interlayer spacing difference of the clays after complete PEO insertion, clay crystallites (tactoids) in the PEO/CX9 nanocomposite may indicate a better dispersion via TEM and steady shear viscosity measurement. With DSC, we observed a fraction of nonintercalated PEO segments with increasing clay loading. The thermal stability of PEO/clay nanocomposites with higher clay content were superior to pure PEO.

From the rheological measurements, an increase in shear viscosity and storage and loss moduli of nanocomposites with clay content were observed. Furthermore, the PEO/CZ nanocomposites with CZ loading exhibit higher zero shear rate viscosities and more rapid shear thinning behavior than pure PEO, which results from reorientation of dispersed clay particles. Surfactant chain length and surface MC also play an importance role in nanocomposite properties (improvement of mechanical properties, heat resistance, and inflammability[57]). These properties depend not only on the polymer−clay characteristics but also on the morphology and interfacial characteristics. The MF equation was used to examine concentration effects on viscosity. The rheological properties of nanocomposite systems depend on clay content and interaction between clay particles. Also, the linear viscoelastic properties appear to be most strongly correlated to the mesoscopic structure, and it is postulated that the molecular weight and interaction strength would affect the mesoscopic structure and the properties of these nanocomposites.

Acknowledgment. This study was supported by research grants from the Korea Science and Engineering Foundation (KOSEF) through the Applied Rheology Center (ARC), an official KOSEF-created engineering research center (ERC) at Korea University, Korea.

References and Notes

(1) Alexandre, M.; Dubois, P. *Mater. Sci. Eng., R* **2000**, *28*, 1.
(2) Giannelis, E. P.; Krishnamoorti, R.; Manias, E. *Adv. Polym. Sci.* **1999**, *138*, 107.
(3) Giannelis, E. P. *Appl. Organomet. Chem.* **1998**, *12*, 675.
(4) Gilman, J. W. *Appl. Clay Sci.* **1999**, *15*, 31.
(5) Gilman, J. W.; Jackson, C. L.; Morgan, A. B.; Harris, R. *Chem. Mater.* **2000**, *12*, 1866.
(6) Bourbigot, S.; Le Bras, M.; Dabrowski, F.; Gilman, J. W.; Kashiwagi, T. *Fire Mater.* **2000**, *24*, 201.
(7) Kim, J. W.; Kim, S. G.; Choi, H. J.; Jhon, M. S. *Macromol. Rapid Commun.* **1999**, *20*, 450.
(8) Kim, J. W.; Noh, M. H.; Choi, H. J.; Lee, D. C.; Jhon, M. S. *Polymer* **2000**, *41*, 1229.
(9) Trlica, J.; Sáha, P.; Quadrat, Q.; Stejskal, J. *Physica A* **2000**, *283*, 337.
(10) Sim, I. S.; Kim, J. W.; Choi, H. J.; Kim. C. A.; Jhon, M. S. *Chem. Mater.* **2001**, *13*, 1243.
(11) Lan, T.; Pinnavaia, T. J. *Chem. Mater.* **1994**, *6*, 2216.
(12) Usuki, A.; Kato, M.; Okada, A.; Kurauchi, T. *J. Appl. Polym. Sci.* **1997**, *63*, 137.
(13) Jeon, H. G.; Jung, H. T.; Lee, S. D.; Hudson, S. *Polym. Bull.* **1998**, *41*, 107.
(14) Giannelis, E. P. *Adv. Mater.* **1996**, *8*, 29.
(15) LeBaron, P. C.; Wang, Z.; Pinnavaia, T. J. *Appl. Clay Sci.* **1999**, *15*, 11.
(16) Aranda, P.; Ruiz-Hitzky, E. *Chem. Mater.* **1992**, *4*, 1395.
(17) Vaia, R. A.; Vasudevan, S.; Krawiec, W.; Scanlon, L. G.; Giannelis, E. P. *Adv. Mater.* **1995**, *7*, 154.
(18) Ogata, N.; Kawakage, S.; Ogihara, T. *Polymer* **1997**, *38*, 5115.
(19) Bajdák, J.; Hackett, E.; Giannelis, E. P. *Chem. Mater.* **2000**, *12*, 2168.
(20) Hackett, E.; Manias, E.; Giannelis, E. P. *Chem. Mater.* **2000**, *12*, 2161.
(21) Solomon, M. J.; Almusallam, A. S.; Seefeldt, K. F.; Somwangthanaroj, A.; Varadan, P. *Macromolecules* **2001**, *34*, 1864.
(22) Pinnavaia, T. J.; Beall, G. W. *Polymer-Clay Nanocomposites*; John Wiley & Sons: London, 2000; p 316.
(23) Lim, Y. H.; Park, O. O. *Macromol. Rapid Commun.* **2000**, *21*, 231.
(24) Reichert, P.; Hoffmann, B.; Bock, T.; Thomann, R.; Mülhaupt, R.; Friedrich, C. *Macromol. Rapid Commun.* **2001**, *22*, 519.
(25) Shin, S. H.; Kim, H. I. *J. Ind. Eng. Chem.* **2000**, *7*, 147.
(26) Krishnamoorti, R.; Giannelis, E. P. *Macromolecules* **1997**, *30*, 4097.
(27) Vaia, R. A.; Giannelis, E. P. *Macromolecules* **1997**, *30*, 7990.
(28) Vaia, R. A.; Giannelis, E. P. *Macromolecules* **1997**, *30*, 8000.
(29) Ogata, N.; Jiménez, G.; Kawai, H.; Ogihara, T. *J. Polym. Sci., Part B: Phys.* **1997**, *35*, 389.
(30) Jiménez, G.; Ogata, N.; Kawai, H.; Ogihara, T. *J. Appl. Polym. Sci.* **1997**, *64*, 2211.
(31) Cho, J. W.; Paul, D. R. *Polymer* **2001**, *42*, 1083.
(32) Jiang, S.; Yu, D.; Ji, X.; An, L.; Jiang, B. *Polymer* **2000**, *41*, 2041.
(33) Kim, B. H.; Jung, J. H.; Kim, J. W.; Choi, H. J.; Joo, J. *Synth. Met.* **2001**, *117*, 115.
(34) Aranda, P.; Ruiz-Hitzky, E. *Acta Polym.* **1994**, *45*, 59.
(35) Krishnamoorti, R.; Vaia, R. A.; Giannelis, E. P. *Chem. Mater.* **1996**, *8*, 1728.
(36) Theng, B. K. G. *The Chemistry of Clay-Organic Reactions*; Halsted Press: New York, 1974.
(37) Galgali, G.; Ramesh, C.; Lele, A. *Macromolecules* **2001**, *34*, 852.
(38) Hoffmann, B.; Dietrich, C.; Thomann, R.; Friedrich, C.; Mülhaupt, R. *Macromol. Rapid Commun.* **2000**, *21*, 57.
(39) Chen, G.; Liu, S.; Zhang, S.; Qi, Z. *Macromol. Rapid Commun.* **2000**, *21*, 746.
(40) Ren, J.; Silva, A. S.; Krishnamoorti, R. *Macromolecules* **2000**, *33*, 3739.
(41) Carreau, P. J.; De Kee, D. C. R.; Chhabra, R. P. *Rheology of Polymeric Systems-Principle and Applications*; Hanser Publishers: Munich, 1997; p 38.
(42) Shin, T. K.; Kim, J.; Choi, H. J.; Jhon, M. S. *J. Appl. Polym. Sci.* **2000**, *77*, 1348.

(43) Park, S. H.; Lim, S. T.; Shin, T. K.; Choi, H. J.; Jhon, M. S. *Polymer* **2001**, *42*, 5737.
(44) Larson, R. G. *The Structure and Rheology of Complex Fluids*; Oxford University Press: New York, 1999; pp 14−15.
(45) Shapiro, A. P.; Probstein, R. F. *Phys. Rev. Lett.* **1992**, *68*, 1422.
(46) Choi, H. J.; Cho, M. S.; Kim, J. W.; Kim, C. A.; Jhon, M. S. *Appl. Phys. Lett.* **2001**, *78*, 3806.
(47) Rosenbaum, E. E.; Hatzikiriakos, S. G.; Stewart, C. W. *Rheol. Acta* **1998**, *37*, 279.
(48) Choi, H. J.; Kim, S. G.; Hyun, Y. H.; Jhon, M. S. *Macromol. Rapid Commun.* **2001**, *22*, 320.
(49) Manias, E.; Hadziioannon, G.; Brinke, T. *Langmuir* **1996**, *12*, 4587.
(50) Schmidt, G.; Nakatani, A. I.; Butler, P. D.; Karim, A.; Han, C. C. *Macromolecules* **2000**, *33*, 7219.
(51) Farris, R. J. *Trans. Soc. Rheol.* **1968**, *12*, 281.
(52) Agarwal, S.; Salovey, R. *Polym. Eng. Sci.* **1995**, *35*, 1241.
(53) Hoffmann, B.; Kressler, J.; Stöppelmann, G.; Friedrich, Chr.; Kim, G.-M. *Colloid Polym. Sci.* **2000**, *278*, 629.
(54) Pignon, F.; Magnin, A.; Piau, J. M.; Cabane, B.; Lindner, P.; Diat, O. *Phys. Rev. E* **1997**, *56*, 3281.
(55) Rohn, C. L. *Analytical Polymer Rheology; Structure Processing Property Relationships*; Hanser Publisher: Munich, 1995; pp 202−204.
(56) Vaia, R. A.; Sauer, B. B.; Tse, O. K.; Giannelis, E. P. *J. Polym. Sci., Polym. Phys.* **1997**, *35*, 59.
(57) Kryszewski, M. *Synth. Met.* **2000**, *109*, 47.

MA002191W